PAPER

Check for updates

New phases of 3d-transition metal–cerium binary compounds: an extensive structural search†

Xiaorui Sun,[a] Yawei Lei,[a] Rulong Zhou, [ID] *[a] Bingyan Qu,[a] Dongdong Li,[a] Bo Zhang[a] and Xiao Cheng Zeng*[bc]

We perform a comprehensive study to explore the low-energy crystalline phases of 3d transitional metal–cerium (TM–Ce) binary compounds using an unbiased structural search method coupled with first-principles optimization. For Ce–Sc, Ce–Ti, Ce–V, Ce–Cr and Ce–Mn binary systems, no stable crystalline phases are found from the structural search, offering an explanation for why none of these binary compounds have been observed in experiments. For Ce–Fe, Ce–Co, Ce–Ni, Ce–Cu and Ce–Zn binary systems, in addition to the previously known experimental structures, we also find several new low-energy crystalline phases. The computed electronic structures show that Ce atoms are in different states in the predicted binary compounds. In the Ce–Fe, Ce–Co and Ce–Ni compounds, the Ce 4f electrons are partially itinerant so that Ce atoms tend to adopt intermediate valence states between Ce^{+4} and Ce^{+3} due to the hybridization among Ce-4f, Ce-5d states and 3d states of TM. In the Ce–Cu and Ce–Zn binary compounds, the Ce-4f states are more localized with the charge state of Ce being close to 3+. In particular, the ferromagnetic metal (FM)-rich phases of the Ce–Fe, Ce–Co and Ce–Ni compounds tend to exhibit FM ordering in their ground states, owing to the strong exchange interaction among metal elements, whereas the non-magnetic states are usually preferred for FM-deficient phases. Magnetic orderings are also found in some other TM-rich phases of Ce–Cu and Ce–Zn compounds, where the magnetic moments are located on the Ce atoms due to the Kondo effect. Mechanic properties of these compounds are also computed based on density functional theory methods. This systematic study offers significantly new data for Ce-based alloys and will be useful to understand the intriguing behavior of the Ce-4f electron, thereby calling for future experimental confirmation of the newly predicted phases of Ce–TM compounds.

1. Introduction

Cerium and cerium-based intermetallic compounds have attracted considerable attention over the past decades due to their rich polymorphs and intriguing physical properties. Ce element itself possesses at least five crystalline phases, denoted as α, α′, β, γ, δ phases, being stable at different conditions.[1,2] One of the most fascinating properties of pure Ce is the γ ⇔ α isostructural solid–solid phase transition at ∼7 kbar.[1,3,4] Not only in Ce crystal, similar phase transitions were also observed in Ce liquid,[5] Ce-based compounds[6] and Ce-based metallic glasses.[7,8] In Ce-based intermetallic compounds, Ce element can exhibit different electronic states, *i.e.* diamagnetic Ce^{4+} ([Xe] $4f^0$), paramagnetic Ce^{3+} ([Xe]$4f^1$), mixed valence or intermediate valence, thereby resulting in diverse properties such as superconductivity,[9,10] heavy-fermion property,[11,12] complex magnetic properties,[13–15] excellent catalytic properties[16–18] and high glass-forming ability,[19,20] *etc.* The ability to adopt a different state for the Ce 4f electron in Ce-based intermetallic compounds leads to an interplay between the Ruderman–Kittel–Kasuya–Yosida (RKKY) interaction and the Kondo effect, as described by the coupling constant J_{cf} that reflects the correlation between the electrons of the open f subshell of Ce and the conduction electrons in the intermetallic compounds.[21] J_{cf} is dependent on temperature, and can be modified by pressure and chemical bonding as well. So different Ce-based intermetallic compounds may exhibit very different properties at different compositions, with different crystal structures and different distances between Ce atoms *etc.*

It is also known that the multi-valence-states of Ce can lead to richer phases of Ce-based intermetallic compounds. For example, for the Ce–Al binary compounds, crystalline phases of Ce_1Al_1,[22] Ce_1Al_2,[23] Ce_1Al_3,[24] Ce_1Al_4 (ref. 25) and Ce_3Al_1 (ref. 26)

[a]Laboratory of Amorphous Matter and Science, School of Materials Science and Engineering, Hefei University of Technology, Hefei, Anhui 230009, China. E-mail: rlzhou@hfut.edu.cn

[b]Department of Chemistry, University of Nebraska-Lincoln, Lincoln, Nebraska 68588, USA. E-mail: xzeng1@unl.edu

[c]Collaborative Innovation Center of Chemistry for Energy Materials, University of Science and Technology of China, Hefei, Anhui 230026, China

† Electronic supplementary information (ESI) available. See DOI: 10.1039/c7ra07103e

were synthesized experimentally, and they exhibit very different physical properties.[27–31] Among all the Ce-based binary compounds, the Ce and transition metal (Ce–TM) are of particular significance due to the interplay between the 4f electrons of Ce and 3d electrons of transition metals, which can lead to rich physical properties. For examples, Ce_1Cu_6 is known to be a heavy-fermion system,[11] while Ce_1Cu_2 exhibits magnetic ordering and Kondo effects.[32] And with the same crystalline structure, Ce_1Co_2 and Ce_1Ni_2 exhibit paramagnetic or non-magnetic property.[33,34] Although considerable efforts have been made for the synthesis of Ce–TM binary compounds in the past decades, only several crystalline phases were successfully synthesized. To date, stable crystal structures of Ce–Sc, Ce–Ti, Ce–V, Ce–Cr and Ce–Mn binary compounds have not been reported in the literature, although some special crystalline structures have been found for the Ce–TM binary compounds, such as Ce_1X_2 and Ce_1X_5 (X = Fe, Co, Ni, Cu, Zn), CeX (X = Ni, Cu, Zn), Ce_1Cu_6 and Ce_1Ni_3 (obtained from Inorganic Crystal Structure Database), *etc.* Much more stable crystalline phases of Ce–TM binary compounds are expected to exist even though they have not been synthesized from experiments. Theoretical predictions of new structures of Ce–TM binary compounds would be helpful to guide future experimental synthesis.

With the state-of-the art global structure search methods, such as genetic algorithm, simulated annealing, topological modeling, and molecular packing, it is possible to identify new crystalline phases of Ce–TM binary compounds. In this study, we perform a systematic search for the stable and low-energy metastable crystalline structures of Ce–TM binary compounds Ce_mTM_n (where TM = Sc, Ti, V, Cr, Mn, Fe, Co, Ni, Cu, Zn) using an evolutionary algorithm combined with first-principles optimization. Besides experimentally observed phases, we found several new low-energy crystalline phases of Ce–TM (TM = Fe, Co, Ni, Cu, Zn). Detailed structures, electronic and mechanical properties of the new phases are described below.

2. Computational method

An unbiased search of stable structures of Ce_mX_n is performed using the USPEX package.[35,36] The selected method is based on an evolutionary algorithm which has been proven to be reliable in identifying new phases of a number of systems.[37–40] The varying composition search method is applied to seek the most optimal composition of each system. Various compositions with the $m : n$ ratios ranging from $1 : 7$ to $7 : 1$ with the constraint of $m + n \leq 8$ are explored. Medium-sized unit cells containing 8–16 atoms are considered. Three hundreds of structures are generated in the first generation which ensures diversity of the structures at each composition. Sixty structures with different compositions are generated in the ensuing generations by using different evolutionary operations to the low-energy structures, including heredity (60% structures), soft mutation (20%), transmutation (10%) and random production (10%). All the structures are optimized using VASP package[41] to achieve medium accuracy. Based on the computed energy of each structure, a rough convex-hull curve of formation energy is plotted, from which possible energetically stable structures and

phases are selected out for further structural optimization at higher accuracy.

The structures which are located on or slightly above the convex-hull are picked out for re-optimization using VASP package. The Perdew–Burke–Enzerhof (PBE)[42] exchange-correlation functional within the generalized gradient approximation (GGA) is used. We will point that although usually a Hubbard U correction should be considered for d- and f-elements, our calculations show that standard GGA calculations can give consistent results with experiments for the Ce–TM binary compounds concerned. Furthermore, GGA without U calculations were also performed in many previous theoretical works about Ce-based intermetallic compounds and also showed great success.[34,43,44] During the structural optimization, an all-electron plane-wave basis set with the energy cutoff of 300 eV and the k-point spacing smaller than $2\pi \times 0.03$ Å^{-1} in the Brillouin zone is used. It is done until the residual force acting on each atom is less than 0.01 eV Å^{-1}. Then more accurate calculations with larger energy cutoff of 600 eV and denser k-point (less than $2\pi \times 0.02$ Å^{-1}) are performed to get more accurate formation energies. Thus, relative stabilities of different structures with the same composition and those with different compositions are found based on the computed convex-hull of formation energy. Furthermore, to assure that no stable phases are missed in the structural search, we also examined structures and phases not seen from the structural search but are stable for other systems. By comparing their formation energies against those structures obtained from the structural search, we can determine the phase stability of each system with more confidence.

To check dynamic stability of all the predicted structures, phonon spectrum, using the finite-displacement approach, is calculated as implemented in the Phonopy code[45] (combined with VASP). Moreover, the elastic constants of all the structures are calculated using the stress–strain relations. Mechanical stabilities of these structures can be examined according to the Born stability criteria.[46–48] From the calculated stiffness constants C_{ij} and the compliance S_{ij}, the Voigt and Reuss bulk and shear moduli are calculated according to the following formula:[49]

$$B_V = \frac{1}{9}[(C_{11} + C_{22} + C_{33}) + 2(C_{12} + C_{23} + C_{31})] \quad (1)$$

$$G_V = \frac{1}{15}[(C_{11} + C_{22} + C_{33}) - (C_{12} + C_{13} + C_{23}) + 3(C_{44} + C_{55} + C_{66})] \quad (2)$$

$$B_R = \frac{1}{(S_{11} + S_{22} + S_{33}) + 2(S_{12} + S_{23} + S_{13})} \quad (3)$$

$$G_R = \frac{15}{4(S_{11} + S_{22} + S_{33}) - (S_{12} + S_{23} + S_{13}) + 3(S_{44} + S_{55} + S_{66})} \quad (4)$$

where B_V, G_V and B_R, G_R are the Voigt bulk and shear moduli, and Reuss bulk and shear moduli respectively. The Voigt and Reuss elastic moduli can be viewed as the upper and lower

bound respectively. In this study, the averaged bulk and shear moduli, $B = (B_V + B_R)/2$ and $G = (G_V + G_R)/2$, are adopted according to Voigt–Reuss–Hill approximations.[49]

3. Results and discussion

3.1 Phase stabilities

We have performed an extensive search for structures of the Ce–TM binary compounds of all 3d transition metals. To determine whether the binary compound of $Ce_{1-x}TM_x$ can be formed and is stable against decomposition into its pure constituents, we calculated the formation enthalpies of all the structures obtained from the search according to the following formula:

$$\Delta H(Ce_{1-x}TM_x) = H(Ce_{1-x}TM_x) - (1-x)H(Ce) - xH(TM)$$

(5)

where $H(Ce_{1-x}TM_x)$, $H(Ce)$ and $H(TM)$ are the enthalpy per atom of the compound $Ce_{1-x}TM_x$, pure Ce and pure TM, respectively. Based on the calculated formation enthalpies, the convex-hull curves of all the systems are plotted, as shown in Fig. 1. The phases which are located at the vertex of the convex-hull are stable to resist decomposition into their pure constituents or phases of other compositions. Before the analysis, dynamic stabilities of the predicted energetically stable phases are examined. As shown in Fig. S1 (see the ESI†), all the predicted energetically stable structures are dynamically stable without any imaginary frequencies. According to the mechanical stability criteria,[46–48] all these phases are also mechanically stable based on the calculated elastic constants listed in Table S1.†

For Ce–Sc, Ce–Ti, Ce–V, Ce–Cr and Ce–Mn, no stable phases were found from the structural search since the formation enthalpies of all the searched structures are positive. So, for TM = Sc, Ti, V, Cr, and Mn, Ce–TM binary compounds are unlikely to form. For Ce–Fe, Ce–Co, Ce–Ni, Ce–Cu and Ce–Zn, interestingly, besides experimentally synthesized phases, some new structures are also found (see Fig. 1), which are also possible to be synthesized because of their low formation enthalpies.

Firstly, for the Ce–Fe binary compounds, a new phase of Ce_1Fe_1-p is found, which is located at the vertex of the convex-hull curve, suggesting its high stability. We also found a phase of Ce_2Fe_1-p whose formation energy lies slightly above the convex-hull curve, similar to Ce_1Fe_2-e and Ce_1Fe_5-e. Since both Ce_1Fe_2-e and Ce_1Fe_5-e are experimentally synthesized, the structure of Ce_2Fe_1-p may also have possibility of being synthesized under certain conditions.

Secondly, for the Ce–Co binary compounds, besides previously synthesized phases of Ce_1Co_2-e and Ce_1Co_5-e, two new phases, Ce_2Co_1-p and Ce_1Co_1-p, are predicted. Ce_2Co_1-p, Ce_1Co_1-p and Ce_1Co_2-e are located at the vertex of the convex-hull of formation energy, while Ce_1Co_5-e lies slightly above. So, Ce_2Co_1-p and Ce_1Co_1-p are also likely to be synthesized.

Thirdly, for the Ce–Ni binary compounds, stable structures Ce_1Ni_1-e, Ce_1Ni_2-e, Ce_1Ni_3-e and Ce_1Ni_5-e have been synthesized experimentally. The experimental structure of Ce_1Ni_3-e cannot

be found from our structural search as it contains 24 atoms in the primitive cell while we constrained the max number of atoms ≤ 16 in the unit cell. The lowest-energy structure of the Ce_1Ni_3-p is 40 meV higher in the formation energy than the experimental structure. Hence the experimental structure of Ce_1Ni_3-e is stable. A new phase of Ce_1Ni_1-p is obtained from the search, which is more than 100 meV lower in the calculated formation energy than the experimental structure. So, Ce_1Ni_1-p is also likely to be synthesized. The experimental phases of Ce_1Ni_3-e and Ce_1Ni_5-e are all located at the vertex of the convex-hull, indicating that these phases are stable. The experiment phase of Ce_1Ni_2-e lies just above the convex-hull curve.

Fourthly, for the Ce–Cu system, three newly predicted structures (Ce_1Cu_1-p, Ce_1Cu_3-p and Ce_1Cu_5-p) along with two synthesized structures (Ce_1Cu_2-e and Ce_1Cu_6-e) give rise to the convex-hull suggesting these predicted structures are also likely to be synthesized.

Lastly, for the Ce–Zn system, stable crystalline compounds with at least five compositions may exist according to the computed convex-hull. The experimental structures of Ce_1Zn_2-e, Ce_1Zn_3-e and Ce_1Zn_5-e are located at the vertex of the convex-hull. The new structure of Ce_1Zn_1-p and Ce_1Zn_7-p are also likely to be synthesized since they are also located at the convex-hull curve. Moreover, a structure of Ce_1Zn_4-p from the search may also be synthesized because its formation energy is very close to the convex-hull curve.

We will point that although extensive efforts have been paid we cannot speculate to find all the possible stable phases of Ce–TM compounds. For some complex phases which include more than sixteen atoms in the primitive cell, and those with too large compositions (x is too big or too small), we cannot find them from our structural search. Nevertheless, so many low-energy phases have been discovered which indicates that our structural search method is efficient. Based on these new phases, as well as those already known phases, we can get deeper understanding on the behavior of the Ce 4f electrons.

3.2 Structural features

The space groups and lattice constants of all the predicted phases are summarized in Table 1. For comparison, the measured lattice constants of the experimental phases are also listed. Clearly, the calculated lattice constants are in good agreement with the measured values for the experimental phases.

3.2.1 Ce–Fe. The experimental phases of Ce_1Fe_2-e and Ce_1Fe_5-e possess high symmetries. Ce_1Fe_2-e belongs to the cubic crystalline system with the space group of $Fd\bar{3}m$ (no. 227). Ce_1Fe_5-e is a hexagonal crystal whose space group is $P6/mmm$ (no. 191). As shown in Fig. 2, in both structures, the Ce and Fe atoms are highly coordinated, forming very compact structures. Here, the coordination number is counted at the bond-length cutoff of 3.5 Å for Ce–Ce bond, 3.2 Å for Ce–Fe bonds and 3.0 Å for Fe–Fe respectively. The same criteria are used when counting the coordination number for the other Ce–TM compounds. In Ce_1Fe_2-e, each Ce atom is in coordination with four Ce atoms and twelve Fe atoms, while each Fe atom is in
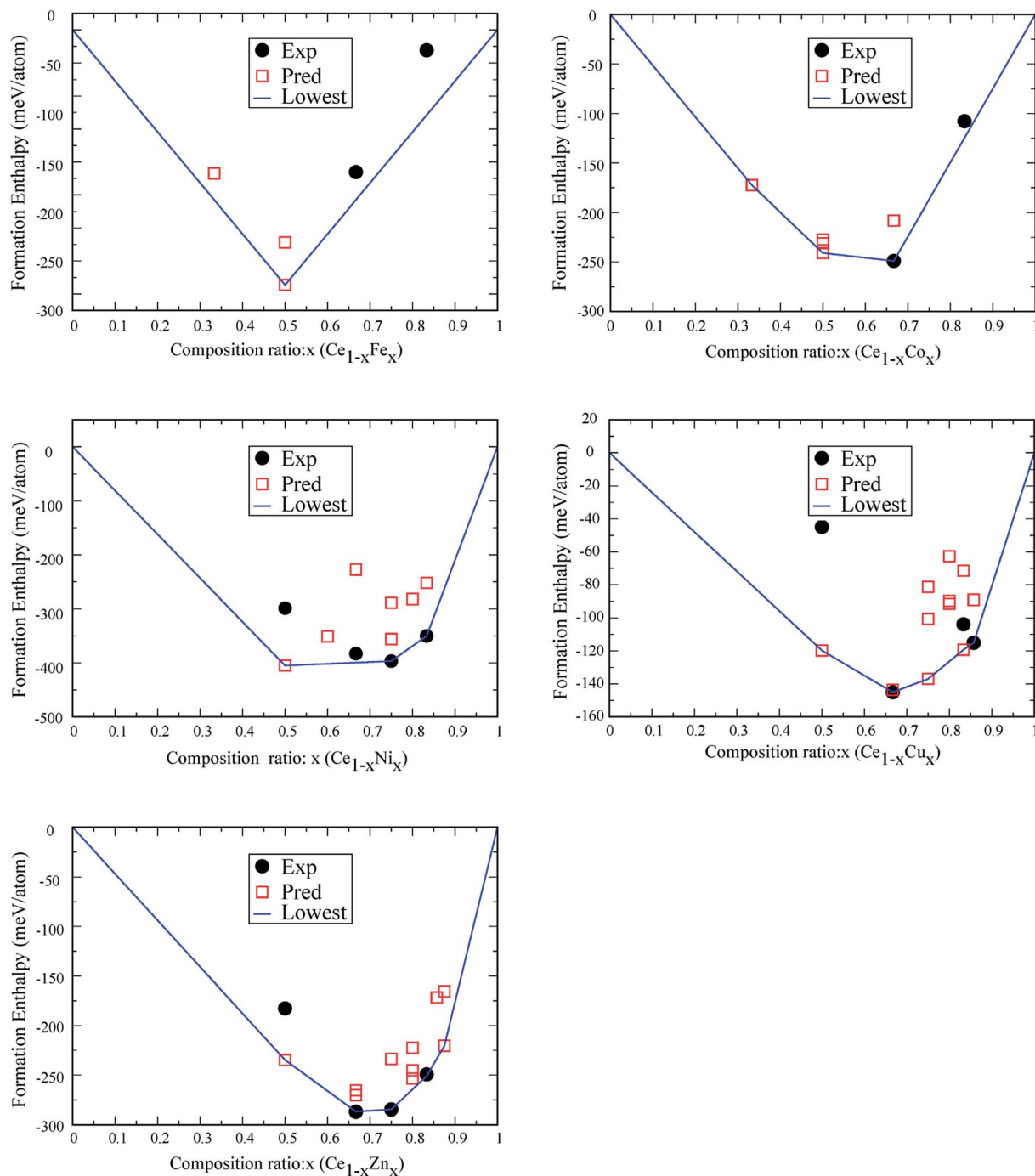
Fig. 1 Convex-hull of formation energies of different Ce−TM binary compounds.

coordination with six Ce atoms and six Fe atoms, forming a distorted icosahedron. In Ce_1Fe_5-e, Ce is in coordination with eighteen Fe atoms, higher than that in Ce_1Fe_2-e. Fe is in coordination with three Ce atoms and nine Fe atoms, the same as that in Ce_1Fe_2-e. In both phases, Fe atoms form tetrahedrons. The Fe tetrahedrons connect with each other *via* sharing the vertex, forming the structural frames. The Ce atoms are inserted into the interstitials of the structural frames.

Structures of the predicted phases Ce_1Fe_1-p and Ce_2Fe_1-p are much different from Ce_1Fe_2-e and Ce_1Fe_5-e. Both structures

possess lower symmetries. Ce_2Fe_1-p is a monoclinic crystal with the space group of $P2_1/m$ (no. 11) while Ce_1Fe_1-p belongs to orthorhombic crystalline system with $Cmcm$ (no. 63) space group. In Ce_2Fe_1-p, there are two nonequivalent Ce atoms in the unit cell. Both are in ten-fold coordination with seven Ce atoms and three Fe atoms. The coordination number of Fe is nine, which includes seven Ce atoms and two Fe atoms. Structurally, Ce_2Fe_1-p can be viewed as Ce bulk with embedded Fe chains. In Ce_1Fe_1-p, each Ce atom is in coordination with seven Fe atoms and four Ce atoms, and each Fe atom is in coordination with

Table 1   The space group, lattice constants, bulk modulus B, shear modulus G, Pugh ratio B/G for Ce–Fe, Ce–Co, Ce–Ni, Ce–Cu, and Ce–Zn compounds

Phases		Space group (no.)	Lattice constant a, b, c (Å) α, β, γ (deg)	B (GPa)	G (GPa)	B/G
Ce$_2$Fe$_1$-p	Cal.	$P2_1/m$ (11)	4.78, 4.72, 5.90 90, 92, 90	51	23	2.22
Ce$_1$Fe$_1$-p	Cal.	$Cmcm$ (63)	4.63, 4.63, 4.48 90, 90, 55	73	25	2.92
Ce$_1$Fe$_2$-e	Cal.	$Fd\bar{3}m$ (227)	5.10, 5.10, 5.10 60, 60, 60	95	19	5.00
	Exp.[a]		5.16, 5.16, 5.16 60, 60, 60		21	
Ce$_1$Fe$_5$-e	Cal.	$P6/mmm$ (191)	4.01, 4.99, 4.99 120, 90, 90	104	58	1.79
	Exp.[a]		4.00, 4.86, 4.86 120, 90, 90			
Ce$_2$Co$_1$-p	Cal.	$C2/m$ (12)	5.91, 5.91, 9.01 131, 131, 35	56	29	1.93
Ce$_1$Co$_1$-p	Cal.	$Cmcm$ (63)	5.88, 5.88, 3.75 90, 90, 36	71	19	3.74
Ce$_1$Co$_2$-e	Cal.	$Fd\bar{3}m$ (227)	4.99, 4.99, 4.99 90, 90, 90	141	32	4.41
	Exp.[a]		5.06, 5.06, 5.06 90, 90, 90			
Ce$_1$Co$_5$-e	Cal.	$P6/mmm$ (191)	4.02, 4.88, 4.88 120, 90, 90	155	49	3.16
	Exp.[a]		4.02, 4.93, 4.93 120, 90, 90	148	42	3.5
Ce$_1$Ni$_1$-p	Cal.	$Fd\bar{3}m$ (191)	4.58, 4.58, 4.58 60, 60, 60	126	66	1.91
Ce$_1$Ni$_2$-e	Cal.	$Fd\bar{3}m$ (227)	5.10, 5.10, 5.10 60, 60, 60	125	47	2.66
	Exp.[a]		5.10, 5.10, 5.10 60, 60, 60			
Ce$_1$Ni$_3$-e	Cal.	$P6_3/mmc$ (194)	4.94, 4.94, 16.55 90, 90, 120	94	52	1.81
	Exp.[a]		4.96, 4.96, 16.53 90, 90, 120			
Ce$_1$Ni$_5$-e	Cal.	$P6/mmm$ (191)	4.89, 4.89, 4.00 90, 90, 120	142	69	2.06
	Exp.[a]		4.89, 4.89, 4.00 90, 90, 120	143	63	2.27
Ce$_1$Cu$_1$-p	Cal.	$Pmma$ (51)	4.45, 3.51, 5.17 90, 90, 90	56	36	1.56
Ce$_1$Cu$_2$-e	Cal.	$Imma$ (74)	5.50, 5.50, 5.50 133, 105, 93	71	27	2.63
	Exp.[a]	$Imma$ (74)	5.60, 5.60, 5.60 133, 102, 96			
Ce$_1$Cu$_3$-p	Cal.	$Cmcm$ (63)	5.23, 5.23, 6.71 90, 90, 47	63	36	1.75
Ce$_1$Cu$_5$-p	Cal.	$F\bar{4}3m$ (216)	5.03, 5.03, 5.03 60, 60, 60	70	45	1.56
Ce$_1$Cu$_6$-e	Cal.	$Pnma$ (62)	8.09, 5.05, 10.14 90, 90, 90	95	29	3.28
	Exp.[a]	$Pnma$ (62)	8.11, 5.10, 10.16 90, 90, 90			
Ce$_1$Zn$_1$-p	Cal.	$Cmcm$ (63)	6.35, 6.35, 4.68 90, 90, 67	43	30	1.43
Ce$_1$Zn$_2$-e	Cal.	$Imma$ (74)	5.72, 5.72, 5.72 133, 105, 93	60	26	2.31
	Exp.[a]	$Imma$ (74)	5.80, 5.80, 5.80 133, 99, 99			

Table 1 (*Contd.*)

| Phases | Space group (no.) | Lattice constant *a*, *b*, *c* (Å) | | | |
		α, β, γ (deg)	*B* (GPa)	*G* (GPa)	*B*/*G*
Ce$_1$Zn$_3$-e	Cal.	*Cmcm* (63)	5.64, 5.64, 6.50	63	42	1.50
			90, 90, 48			
	Exp.[a]	*Cmcm* (63)	5.71, 5.71, 6.64			
			90, 90, 48			
Ce$_1$Zn$_4$-p	Cal.	*I*4/*mmm* (139)	6.01, 6.01, 6.01	69	29	2.38
			138, 138, 60			
Ce$_1$Zn$_5$-e	Cal.	*P*6/*mmm* (191)	5.37, 5.37, 4.26	78	43	1.81
			90, 90, 120			
	Exp.[a]		5.39, 5.39, 4.27			
			90, 90, 120			
Ce$_1$Zn$_7$-p	Cal.	*Cmmm* (65)	6.07, 6.07, 5.75	68	41	1.66
			60, 60, 139			

[a] Lattice constants derived from Inorganic Crystal Structure Database.
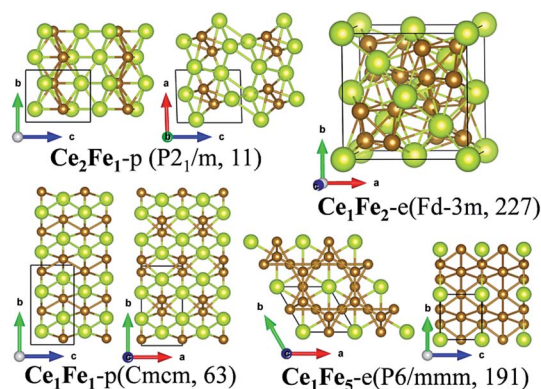
Fig. 2 Crystalline structures of Ce$_2$Fe$_1$-p, Ce$_1$Fe$_1$-p, Ce$_1$Fe$_2$-e and Ce$_1$Fe$_5$-e. The new predicted phases are denoted as Ce$_m$Fe$_n$-p, while those taken from in experiments are denoted as Ce$_m$Fe$_n$-e. And so does for Ce–Co, Ce–Ni, Ce–Cu and Ce–Zn compounds.

seven Ce atoms and two Fe atoms. The coordination number of Ce is a little higher than that in Ce$_2$Fe$_1$-p while the coordination number of Fe in both structures is the same. Fe atoms also form Fe chains similar as those in Ce$_2$Fe$_1$-p. So, Ce$_2$Fe$_1$-p and Ce$_1$Fe$_1$-p also exhibit some similarity in structures, similar as Ce$_1$Fe$_2$-e and Ce$_1$Fe$_5$-e. It seems that the richness of Fe dominants general structural features of Ce–Fe binary compounds.

3.2.2 Ce–Co. For Ce–Co compounds, stable phases are also found for the composition of Ce$_2$Co$_1$-p, Ce$_1$Co$_1$-p, Ce$_1$Co$_2$-e and Ce$_1$Co$_5$-e, same as Ce–Fe compounds. The experimental phases of Ce$_1$Co$_2$-e and Ce$_1$Co$_5$-e are also the most energetically stable phases for these compositions. Their structures are the same as the corresponding phases of Ce–Fe compounds (see Fig. 3). The structures of the predicted phases of Ce$_2$Co$_1$-p and Ce$_1$Co$_1$-p are similar to those of Ce–Fe compounds with a little difference. Ce$_2$Co$_1$-p is a monoclinic crystal with the space group of *C*2/*m* (no. 12). Its structure is very loose, compared to Ce$_2$Fe$_1$-p. The coordination number of Ce$_1$, Ce$_2$ and Co is six, seven and seven, respectively, all apparently less than those of Ce$_2$Co$_1$-p. The average bond lengths of Ce–Ce and Ce–Co in Ce$_2$Co$_1$-p are

longer than those in Ce$_1$Co$_2$-e. The structure of Ce$_1$Co$_1$-p is similar to that of Ce$_1$Fe$_1$-p. Compared to Ce$_1$Fe$_1$-p, the structure of Ce$_1$Co$_1$-p is elongated along the crystal basis vector $\vec{b}$, causing decreased Ce–Ce bonds and Ce–Co bonds. So, in Ce$_1$Co$_1$-p, the coordination number of Ce and Co is seven and nine, respectively, less than those in Ce$_1$Fe$_1$-p as well.

3.2.3 Ce–Ni. For the four stable phases of Ce–Ni binary compounds, the experimental structures of Ce$_1$Ni$_2$-e and Ce$_1$Ni$_5$-e are the same as those of Ce–Fe and Ce–Co compounds (see Fig. 4). The experimental structure Ce$_1$Ni$_3$-e possesses a hexagonal lattice with the space group of *P*6$_3$/*mmc* (no. 194). There are two nonequivalent Ce atoms (denoted as Ce$_1$ and Ce$_2$ respectively) and four nonequivalent Ni atoms in each unit cell, respectively. The first Ce atom (Ce$_1$) is located at the center of a hexagonal ring of six Ni atoms. Besides the six Ni atoms, Ce$_1$ is bonded with two Ce$_2$ atoms located directly above and below Ce$_1$. So the coordination number of Ce$_1$ is eight. Ce$_2$ is bonded with one Ce$_1$ atom, three Ce$_2$ atoms and twelve Ni atoms, respectively, and has a high coordination number of sixteen. For Ni atoms, the coordination number of three of them is twelve, while that of others is ten.

The structure of the predicted phases Ce$_1$Ni$_1$-p is much different from the experimental one and possesses much lower energy. Ce$_1$Ni$_1$-p has a cubic lattice with the space group of *Fd*$\bar{3}$*m* (no. 227). Each Ce or Ni atom is located at the center of a cubic whose vertices are occupied by four Ce or four Ni atoms,
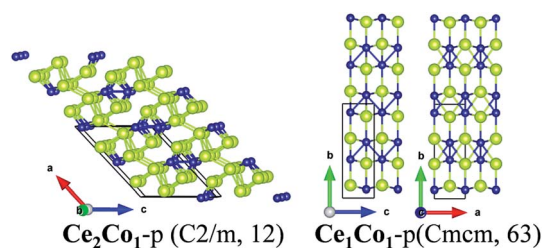

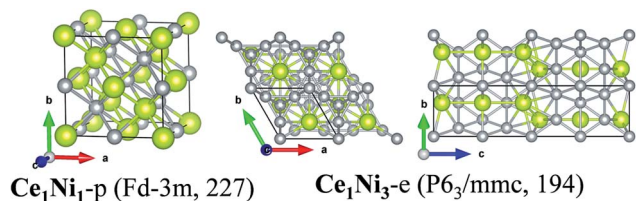
Fig. 3 Crystalline structures of Ce$_2$Co$_1$-p and Ce$_1$Co$_1$-p.

Ce$_1$Ni$_1$-p (Fd-3m, 227)   **Ce$_1$Ni$_3$-e** (P6$_3$/mmc, 194)

Fig. 4 Crystalline structures of Ce$_1$Ni$_1$-p and Ce$_1$Ni$_3$-e.

respectively. The four Ce atoms at the cubic vertices form regular tetrahedron, and so do the four Ni atoms. Thus, both Ce and Ni are in eight-fold coordination.

3.2.4 Ce–Cu. For Ce–Cu binary compounds, four experimental phases are reported, namely, Ce$_1$Cu$_1$-e, Ce$_1$Cu$_2$-e, Ce$_1$Cu$_5$-e and Ce$_1$Cu$_6$-e. Ce$_1$Cu$_2$-e and Ce$_1$Cu$_6$-e are the most energetically stable phases of their compositions, based on our calculation. However, Ce$_1$Cu$_1$-e and Ce$_1$Cu$_5$-e are only metastable because a new phase with much lower formation enthalpy for each composition is found from our unbiased search. The structure of Ce$_1$Cu$_5$-e is the same as that of Ce$_1$Fe$_5$-e, Ce$_1$Co$_5$-e and Ce$_1$Ni$_5$-e. No stable phases are found for Ce$_1$TM$_6$ for other transition metals. Although Ce$_1$Cu$_2$-e is still very stable, its structure is much different from those of Ce$_1$Fe$_2$-e, Ce$_1$Co$_2$-e and Ce$_1$Ni$_2$-e. As shown in Fig. 5, Ce$_1$Cu$_2$-e possesses an orthorhombic lattice and belongs to *Imma* (no. 74) space group, while Ce$_1$Fe$_2$-e, Ce$_1$Co$_2$-e and Ce$_1$Ni$_2$-e are all cubic crystals with space group of *Fd$\bar{3}$m* (no. 227). Ce$_1$Cu$_2$-e can be viewed as constructed by inserting Ce atoms between buckled Cu honeycomb slabs. Ce atoms are located directly above the center of all the hexagonal rings. The coordination number of Ce and Cu in Ce$_1$Ni$_2$-e is 14 and 10, respectively, both being a little less than that in Ce$_1$Fe$_2$-e, Ce$_1$Co$_2$-e and Ce$_1$Ni$_2$-e.

For the predicted phases, Ce$_1$Cu$_1$-p possesses an orthorhombic crystalline lattice with space group of *Pmma* (no. 51). Both Ce and Cu atoms form zig-zag atomic chains, respectively. Each Ce atomic chain connects with four Cu atomic chains, and *vice versa*. Each Ce atom is in coordination with six Cu atoms and two Ce atoms, and each Cu atom is in coordination with six
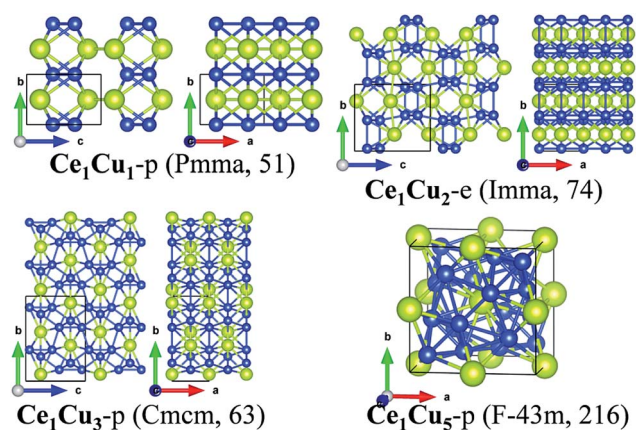
Ce atoms and two Cu atoms. So the coordination number of them is eight. Ce$_1$Cu$_5$-p is a cubic crystal with the space group of *F$\bar{4}$3m* (no. 216). In the conventional cell, there are one Ce atom located at the center of the cube and one Ce atom located at the center of each side of the cube, respectively. The Cu atoms form a face-capped pyramid structure with the Ce atom at the center. The four vertexes of the pyramid point to the four non-nearest-neighbor corners of the cube to keep the T_d rotation symmetry of the structure. The central Ce atom is bonded with all the Cu atoms of the face-capped pyramid except the four corner ones. Thus its coordination number is 16. The 16 Cu atoms coordinated with the Ce atom form a polyhedron with 28 faces. There are 4 hexagons and 12 pentagons in this 28-faces polyhedron. Each Cu atom is in 12-fold coordination, giving a distorted icosahedron with the surrounded atoms. The local structure of Ce$_1$Cu$_5$-p is a little similar to those of Ce$_1$Fe$_2$-e, Ce$_1$Co$_2$-e and Ce$_1$Ni$_2$-e, where the 28-faces polyhedron and icosahedron are also formed with the center of Ce and the transition atom respectively.

3.2.5 Ce–Zn. For Ce–Zn binary compounds, four phases are reported in the literatures, namely, Ce$_1$Zn$_1$-e, Ce$_1$Zn$_2$-e, Ce$_1$Zn$_3$-e and Ce$_1$Zn$_5$-e. According to our calculation, Ce$_1$Zn$_2$-e, Ce$_1$Zn$_3$-e and Ce$_1$Zn$_5$-e are indeed the most energetically stable structures of the corresponding compositions, while Ce$_1$Zn$_1$-e is not. The structure of Ce$_1$Zn$_5$-e is the same as those of Ce$_1$Fe$_5$-e, Ce$_1$Co$_5$-e, Ce$_1$Ni$_5$-e and Ce$_1$Cu$_5$-e. Ce$_1$Zn$_2$-e is very similar to that of Ce$_1$Cu$_2$-e (Fig. 6). Both structures have the same space group of *Imma* (no. 74). Zn atoms form buckled single-layer honeycomb slabs as Cu atoms do in Ce$_1$Cu$_2$-e. Ce atoms are located above the center of each hexagonal ring. The buckling of Zn honeycomb slabs is more dramatic than that of the Cu honeycomb slabs in Ce$_1$Cu$_2$-e, due to the shorter Zn–Zn bonds connecting adjacent bucking Zn honeycomb slabs. Ce$_1$Zn$_3$-e has the same space group as Ce$_1$Cu$_3$-p. After checking the detailed structures
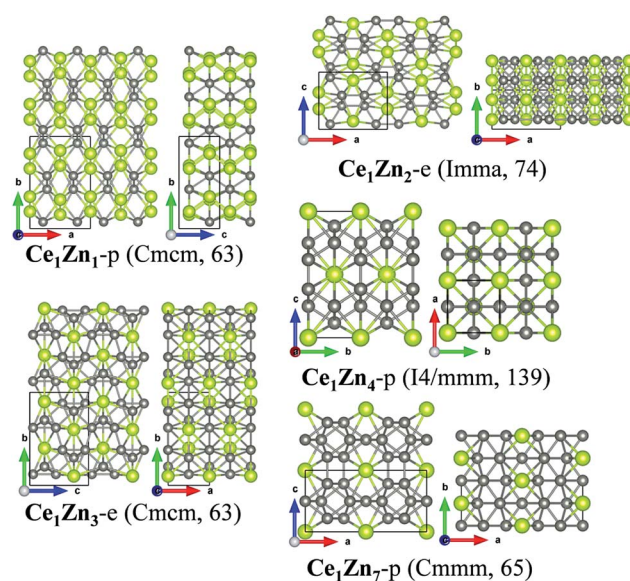

Ce$_1$Cu$_1$-p (Pmma, 51)   **Ce$_1$Cu$_2$-e** (Imma, 74)

Ce$_1$Cu$_3$-p (Cmcm, 63)   **Ce$_1$Cu$_5$-p** (F-43m, 216)

Fig. 5 Crystalline structures of Ce$_1$Cu$_1$-p, Ce$_1$Cu$_2$-e, Ce$_1$Cu$_3$-p and Ce$_1$Cu$_5$-p.

Ce$_1$Zn$_1$-p (Cmcm, 63)   **Ce$_1$Zn$_2$-e** (Imma, 74)

Ce$_1$Zn$_3$-e (Cmcm, 63)   **Ce$_1$Zn$_4$-p** (I4/mmm, 139)

Ce$_1$Zn$_7$-p (Cmmm, 65)

Fig. 6 Crystalline structures of Ce$_1$Zn$_1$-p, Ce$_1$Zn$_2$-e, Ce$_1$Zn$_3$-e, Ce$_1$Zn$_4$-p and Ce$_1$Zn$_7$-p.

of Ce_1Zn_3-e and Ce_1Cu_3-p, we find that they are almost the same. The success of the synthesis of Ce_1Zn_3-e implies that the synthesis of Ce_1Cu_3-p is also possible to be synthesized by experiment.

For the predicted phases, the structure of Ce_1Zn_1-p is the same as that of Ce_1Fe_1-p and is similar to that of Ce_1Co_1-p. Ce_1Zn_4-p is metastable according to the computed formation energy. It is a tetragonal crystal with the space group of $I4/mmm$ (no. 139). Each Ce atom is encapsulated by a cage constructed by 18 Zn atoms. The four sides of the Zn cage are all hexagonal rings, while the two roofs are both constructed by four rhombic rings. The coordination number of Ce is 16 and that of Zn is 8. Ce_1Zn_7-p possesses an orthorhombic crystalline structure and the space group of $Cmmm$ (no. 65). Its structure is much more complicated because there are more atoms included in one conventional unit cell. All the Ce atoms are equivalent in crystallography, while there are three nonequivalent Zn atoms. Each Ce atom is in coordination with 12 Zn atoms. Zn_1, Zn_2, and Zn_3 have a coordination number of 9, 8 and 10, respectively.

3.3 Electronic properties

The diverse physical properties such as heavy-fermion, Kondo-lattice, and intermediate-valence effects of Ce-based binary compounds are highly correlated with the behavior of the 4f electrons in Ce. For the Ce–TM binary compounds, the 3d electrons of the TM elements may also affect their properties. To compute their electronic structures, various initial arrangements of magnetic moments, such as the ferromagnetic, anti-ferromagnetic, were considered for each structure and the spin-polarized (SP) calculations were performed for each magnetic configuration. We also carried out a non-spin-polarized (NSP) for each structure to compute the energy of a spin-degenerate nonmagnetic phase. The optimized stable magnetic configurations, the magnetic moment on each atom, and the relative energy per atom of the ferro- or antiferro-magnetic configurations compared to that of the spin-degenerate nonmagnetic state of each structure, are all listed in Table 2. To gain deeper insight into the electronic and magnetic structures, the projected density of state (PDOS) of each phase is calculated, as shown in Fig. S2–S6 (see the ESI†).

From the computed PDOS, we can see that there is obvious hybridization between the 3d states of the TM elements and the 4f and 5d states of Ce atoms for the Ce–Fe, Ce–Co and Ce–Ni binary compounds, while that for the Ce–Cu and Ce–Zn binary compounds is much weaker. Due to the strong hybridization, the distribution of the Ce 4f states is apparently broadened for Ce–Fe, Ce–Co and Ce–Ni compounds. For some phases, the Ce 4f states distribute in very large energy windows (3 to 4 eV) below the Fermi level, which means that some 4f electrons of Ce become itinerant, i.e. the Ce atoms may adopt intermediate valence states in these phases. For the Ce–Cu, Ce–Zn systems, the close-shell features of the 3d orbitals of Cu and Zn render them far away from the 4f orbitals of Ce. Hence, there is little hybridization between them. As shown in Fig. S5 and S6,† the density of the 4f states of Ce in the Ce–Cu and Ce–Zn compounds is quite localized, and is crossed by E_F in their lower

part, indicating that the lower 4f bands are filling by electrons. In almost all the phases of Ce–Cu and Ce–Zn systems, the Ce atoms adopt trivalent states.

Moreover, as shown in Fig. S2–S6,† spin splitting occurs for some phases e.g. Ce_1Fe_2-e, Ce_1Fe_5-e, Ce_1Co_5-e, Ce_1Ni_5-e, etc., suggesting that particular magnetic orderings are energetically favored in these phases. We will discuss these ordered magnetic states in details in the following subsections.

3.3.1 Ce–Fe. First, we compare our results with the experimental measurements or previous theoretical calculations. Previous experiment[50] and theoretical calculation[43] have shown that Ce_1Fe_2-e possesses an ferromagnetic configuration in which the magnetic moments of all the Fe atoms are in the same direction (so do the Ce atoms), while the direction of magnetic moments of the Ce atoms is opposite to that on the Fe atoms. To obtain the ground magnetic state of Ce_1Fe_2-e, we consider five different initial spin arrangements (i.e. ↑↑·↑↑↑↑, ↓↓·↑↑↑↑, ↑↓·↓↓↓↓, ↑↑·↑↓↑↓, ↑↓·↑↓↑↓) in spin-polarized calculation and non-spin-polarized calculation to simulate the spin-degenerate nonmagnetic state. The initial magnetic moments on Ce and Fe are both 4 μ_B, and so do for the other compounds. After structural and electronic relaxation, two magnetic configurations are stable and listed in Table 2. The ground magnetic state is ↓↓·↑↑↑↑, consistent with previous experimental and theoretical results. The next energetically stable magnetic state is ↓↓·↑↓↑↓, i.e. the moments on the Fe atoms are aligned anti-ferromagnetically while magnetic moments on Ce atoms adopt the same direction. The highest energy state is the nonmagnetic state. The relative energies of the ground state and the first excited state with respect to the nonmagnetic state are −94 meV per atom and −27 meV per atom, respectively. The large energy difference between the ferromagnetic state and the nonmagnetic state indicates that the ferromagnetic state of Ce_1Fe_2-e is quite stable.

From the computed projected magnetic moments, we can see that in the ground magnetic state of Ce_1Fe_2-e, the magnetic moment (1.76 μ_B) of Fe atoms is almost entirely originated from the 3d states, whereas that of Ce atoms is originated from both 4f (−0.58 μ_B) states and 5d (−0.23 μ_B) states. From the PDOS shown in Fig. S2,† we can see that almost all of the spin-up Fe 3d states are distributed below the Fermi level, meaning that they are almost full-filled, while the spin-down Fe 3d states distribute a little higher and some of them are located above the Fermi level. Thus, the net magnetic moments on Fe atoms are aligned upward. Moreover, because the overlapping of the spin-down Fe 3d states with the Ce 4f and 5d states, there is strong hybridization between them, which results in more Ce 4f and 5d electrons occupying the spin-down states. So the net magnetic moments on Ce atoms are aligned opposite to those on Fe atoms.

For the Ce_1Fe_5-e, spin-polarized computations with ten initial magnetic configurations (i.e. ↑·↑↑↑↑↑, ↑·↓↑↑↑↑, ↓·↓↑↑↑↑, ↑·↑↓↑↑↑, ↑·↓↓↑↑↑, ↓·↓↓↑↑↑, ↑·↑↓↓↑↑, ↑·↓↓↑↑↑, ↓·↓↓↑↑↑, ↓·↑↓↑↑↓), and non-spin-polarized calculation are performed. Three differently ordered magnetic configurations are found to be stable after relaxation. The most stable magnetic configuration is still ferromagnetic (↓·↑↑↑↑↑), as

Table 2 Magnetic properties of Ce–Fe, Ce–Co, Ce–Ni, Ce–Cu, and Ce–Zn compounds. The ↑, ↓ and O represent the positive, negative and zero magnetic moment, respectively. The signs (↑, ↑ or O) before and behind the dot represent the directions of the magnetic moments on Ce and TM (TM = Fe, Co, Ni) atoms respectively. For the Ce–Cu and Ce–Zn compounds, the signs for Cu or Zn are omitted since the magnetic moment on Cu or Zn is always zero. The relative energies ΔE (in meV per atom) of magnetic ordering state compared to that of the spin-degenerate nonmagnetic state are also calculated and shown in the table

Phase	Ground magnetic state	First excited magnetic state	Second excited magnetic state
Ce_2Fe_1-p	Nonmagnetic		
Ce_1Fe_1-p	Nonmagnetic		
Ce_1Fe_2-e	↓↓·↑↑↑↑	↓↓·↑↓↑↓	Nonmagnetic
	Ce: −0.83	Ce: −0.33	
	Fe: 1.76	Fe: 1.45 (−0.22)	
ΔE	−94	−27	
Ce_1Fe_5-e	↓·↑↑↑↑↑	↓·↓↑↑↑↑	↑·↓↓↓↑↑
	Ce: −0.61	Ce: −0.38	Ce: 0.17
	Fe: 2.12	Fe: −0.88 (1.97)	Fe: −1.78(1.40)
ΔE	−203	−110	−97
Ce_2Co_1-p	Nonmagnetic		
Ce_1Co_1-p	Nonmagnetic		
Ce_1Co_2-e	Nonmagnetic		
Ce_1Co_5-e	↓·↑↑↑↑↑	O·↑↓OOO	Nonmagnetic
	Ce: −0.74	Ce: 0.0	
	Co: 1.40	Co_1: 0.55(−0.55); Co_2: 0.0	
ΔE	−69	−1	
Ce_1Ni_1-p	Nonmagnetic		
Ce_1Ni_2-e	Nonmagnetic		
Ce_1Ni_3-e	Nonmagnetic		
Ce_1Ni_5-e	↓·↑↑↑↑↑	Nonmagnetic	
	Ce: −0.23		
	Ni_1: 0.18; Ni_2: 0.26		
ΔE	−3		
Ce_1Cu_1-p	Nonmagnetic		
Ce_1Cu_2-e	↑↓	Nonmagnetic	
	Ce: 0.08 (−0.08)		
ΔE	−2		
Ce_1Cu_3-p	↓↓	Nonmagnetic	
	Ce: −0.23		
ΔE	−0.07		
Ce_1Cu_5-p	↓	Nonmagnetic	
	Ce: −0.21		
ΔE	−0.1		
Ce_1Cu_6-e	↓↓↓↓	↓↑↑↑	↓↓↑↑
	Ce: −0.33	Ce: −0.13(0.27)	Ce: 0.23 (−0.23)
ΔE	−0.18	−0.02	−0.00
Ce_1Zn_1-p	Nonmagnetic		
Ce_1Zn_2-e	↑↑	↑↓	Nonmagnetic
	Ce: 0.65	Ce: 0.42(−0.42)	
	−6.8	−0.5	
Ce_1Zn_3-e	↑↓	Nonmagnetic	
	Ce: 0.34 (−0.34)		
ΔE	−1		
Ce_1Zn_4-p	↑	Nonmagnetic	
	Ce: 0.64		
ΔE	−3		
Ce_1Zn_5-e	↑	Nonmagnetic	
	Ce: 0.73		
ΔE	−3		
Ce_1Zn_7-p	↑	Nonmagnetic	
	Ce: 0.63		
ΔE	−2		

that of Ce_1Fe_2-e. The magnetic moments on Ce atoms are $-0.61\ \mu_B$ and those on Fe atoms are $2.12\ \mu_B$. The magnetic moments on Ce are also contributed by both Ce 4f and 5d electrons. As shown in Fig. S2,† similar to Ce_1Fe_2-e, the reason

for the magnetic moments on Ce atoms is the strong hybridization between the Fe 3d and Ce 4f and 5d states due to the large splitting of the 3d spin-up and spin-down states. The energy difference between the ferromagnetic state and the

nonmagnetic state is −203 meV per atom. Hence, the ferromagnetic state is quite stable. Besides the ferromagnetic state, two magnetic states, *i.e.* ↓·↓↑↑↑↑ and O·↓↓↓↑↑ are metastable with the energy differences of −110 meV per atom and −97 meV per atom with respect to the nonmagnetic state, respectively. Because of the large energy difference, the two magnetic states are also stable.

For the two predicted Ce–Fe phases, Ce_2Fe_1-p and Ce_1Fe_1-p, although various initial magnetic configurations are considered, all of them converge into the nonmagnetic state. It is known that with the large positive value of the exchange interaction J between Fe atoms, bulk Fe and Fe-rich alloys tend to exhibit ferromagnetic properties. As discussed above, for the Fe-rich Ce–Fe phases (Ce_1Fe_2-e and Ce_1Fe_5-e), each Fe atom is in coordination with many Fe atoms (six and nine for Ce_1Fe_2-e and Ce_1Fe_5-e, respectively). The strong exchange interaction renders the moments on the Fe atoms aligned in the same direction. Therefore, Ce_1Fe_2-e and Ce_1Fe_5-e exhibit ferromagnetic properties in the ground state. In the phases of Ce_2Fe_1-p and Ce_1Fe_1-p, each Fe atom is only in coordination with two Fe atoms. The exchange interaction between Fe atoms is much weaker compared to those in the Fe-rich phases of Ce–Fe compounds. Such a weak exchange interaction between Fe atoms cannot force the electron spins of all the Fe atoms aligned in the same direction. As a result, there is no spin splitting of 3d states of Fe for Ce_2Fe_1-p and Ce_1Fe_1-p phases. As seen in Fig. S2,† although no splitting between the spin-up and the spin-down states, the hybridization between the Fe 3d states and the Ce 4f and 5d states is also obvious. The Ce atoms in the Ce_2Fe_1-p and Ce_1Fe_1-p also adopt intermediate valence states, *i.e.* some 4f electrons of Ce are itinerant.

3.3.2 Ce–Co.

For the Ce–Co compounds, only Ce_1Co_5-e exhibits ordered magnetic properties as shown in Table 1 and Fig. S3.† The arrangement of the magnetic moments of the ground magnetic state of Ce_1Co_5-e is the same as that of Ce_1Fe_5-e, but with less negative relative energy (−69 meV per atom) with respect to the nonmagnetic state. This result is easy understood because the structures of Ce_1Co_5-e and Ce_1Fe_5-e are the same and the magnetic properties of Co are similar to those of Fe but with weaker exchange interaction for Co than Fe. Besides the ground ferromagnetic state, there is also a metastable ordered magnetic state for Ce_1Co_5-e which is O·↑↑↓OOO (ferrimagnetic). Its relative energy with respect to the nonmagnetic state is −1 meV per atom, and much smaller (in absolute value) than that of the ferromagnetic state. Because the relative energy of the ferrimagnetic state with respect to the spin-degenerate nonmagnetic state is very small, it should be not stable even at very low temperature.

The ground states of Ce_2Co_1-p, Ce_1Co_1-p and Ce_1Co_2-e are all nonmagnetic (same for spin-polarized calculation and non-spin-polarized calculation). Note that the structure of Ce_1Co_2-e is the same as that of Ce_1Fe_2-e. The nonmagnetic ground state of Ce_1Co_2-e is surely due to the weak exchange interaction of Co. From Fig. S3† we can see that the PDOS of Ce_2Co_1-p, Ce_1Co_1-p and Ce_1Co_2-e are similar to that of the corresponding Ce–Fe phases except the non-spin-splitting. The distance between the main distribution of the 3d states of the TM and that of the 4f

states of Ce is a little larger for Ce_2Co_1-p and Ce_1Co_1-p phases than the corresponding Ce–Fe phases. Thus, the hybridization between the Co 3d states and the Ce 4f states is weaker in both Ce–Co phases than the Ce–Fe phases. For the Ce–Co phases, the hybridization between the Co 3d states and the Ce 4f states is still strong although there is no spin-splitting in the 3d states. So in the Ce–Co phases, the Ce 4f electrons are also partial itinerant.

3.3.3 Ce–Ni.

For the Ce–Ni compounds, the electronic structures are similar to those of Ce–Co systems. Only Ce_1Ni_5-e exhibits ordered magnetic patterns, and it is also ferromagnetic. This is discrepancy with experiment, which is also encountered in the theoretical study.[34] However, this must be regard as a minor one since the energy difference between the ferromagnetic state and the nonmagnetic state is only −3 meV per atom. The Ce_1Ni_1-p, Ce_1Ni_2-e and Ce_1Ni_3-e adopt nonmagnetic ground state based on our calculations. The Ce atoms in the phases of Ce_1Ni_2-e, Ce_1Ni_3-e and Ce_1Ni_5-e also adopt intermediate valence states due to the hybridization between the Ce-4f states and Ni-3d states as shown in Fig. S4.†

Very interestingly, as shown in Fig. S4,† there is an energy gap in which the Fermi level is located for the phase of Ce_1Ni_1-p, meaning that it is a semiconductor rather than a conductor. Its band structure is shown in Fig. 7. The computed band gap is 0.15 eV at PBE level. To verify the existence of the band gap, we also used the Heyd–Scuseria–Ernzerhof (HSE06) exchange-correlation functional.[51] The computed HSE06 band gap is very close to the PBE value. From the PDOS, we see that the top of the valence band and the bottom of the conduction band are both mainly contributed by Ce-4f states. The appearance of the band gap at E_F suggests that all the Ce-4f electrons become conducting electrons, *i.e.* they are delocalized. Thus, in the phase Ce_1Ni_1-p, the Ce atoms are in tetravalent state which is different from all the other phases of Ce–TM compounds.

3.3.4 Ce–Cu and Ce–Zn.

For the Ce–Cu compounds, Ce_1Cu_2-e, Ce_1Cu_3-p, Ce_1Cu_5-p, Ce_1Cu_6-e possess magnetic properties in their ground states. As listed in Table 2 and shown in Fig. S5,† the magnetic moments are only originated from Ce atoms in these Ce–Cu phases. Ce_1Cu_2-e is in antimagnetic state, consistent with the experiment,[32] while Ce_1Cu_3-p, Ce_1Cu_5-p and Ce_1Cu_6-e are both in ferromagnetic states. Note that the energy difference between the ordered magnetic state and the nonmagnetic state for each phase is negligibly small. Thus, the magnetic properties can only be kept stable at extremely low temperature. Kondo effect may be responsible for the magnetic moments on Ce atoms since they are all Cu-rich phases. For Ce_1Cu_1-p, it's in a nonmagnetic ground state.

The magnetic properties of Ce–Zn compounds are similar to those of Ce–Cu compounds. Ce_1Zn_2-e, Ce_1Zn_3-e, Ce_1Zn_4-p, Ce_1Zn_5-e and Ce_1Zn_7-p possess magnetic properties in their ground states. Ce_1Zn_3-e is in the antiferromagnetic state while Ce_1Zn_2-e, Ce_1Zn_4-p, Ce_1Zn_5-e and Ce_1Zn_7-p are all in ferromagnetic states. As in Ce–Cu system, the energy differences between ground magnetic state and nonmagnetic state for Ce_1Zn_2-e, Ce_1Zn_3-e, Ce_1Zn_4-p, Ce_1Zn_5-e and Ce_1Zn_7-p are also small. The reason for the magnetic properties of the Zn-rich
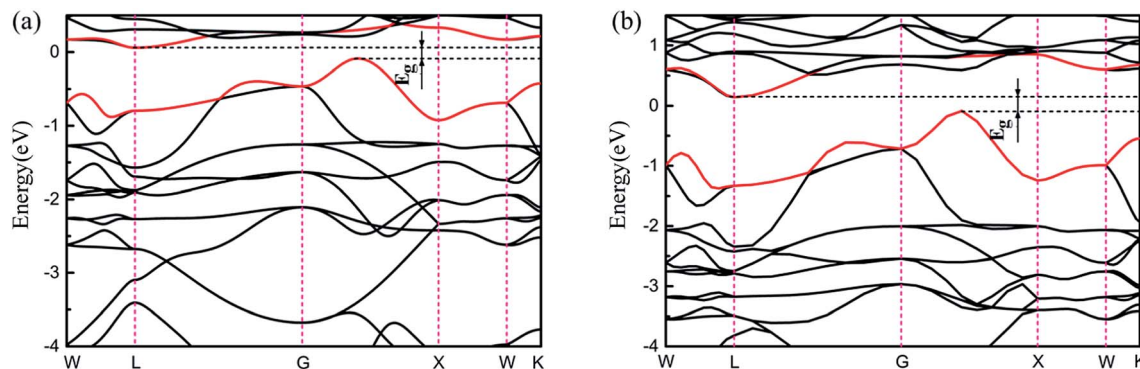
Fig. 7 (a) and (b) are the band structure of the Ce_1Ni_1-p phase using PBE and HSE06 functional, respectively.

phases is also the Kondo effect. For Ce_1Zn_1-p, its ground magnetic state is nonmagnetic state.

3.4 Mechanical properties

Considering the potential application of the Ce–TM compounds, we also computed their mechanical properties. The computed bulk modulus B and shear modulus G are listed in Table 1. Detailed elastic constants are listed in Table S1 (see the ESI†). Based on the bulk modulus and shear modulus, Pugh[52] introduced a parameter B/G to distinguish whether the material is ductile or brittle. When the value of B/G is greater than 1.75, this material is ductile, otherwise it is brittle. The values of B/G for each phase are also listed in Table 1.

As listed in Tables 1 and S1,† the calculated elastic constants and moduli of some experimental phases are in excellent agreement with the measured values.[53–56] Because Ce is a much softer material compared to the 3d transition metals, the bulk moduli of Ce–TM compounds will increase as the concentration of the TM elements increases, as listed in Table 1. Among these different Ce–TM compounds, Ce–Co and Ce–Ni compounds usually possess larger bulk moduli than the same composition Ce–Fe, Ce–Cu and Ce–Zn compounds. The bulk modulus reflects the ability of a substance resisting the compression, and it is in relation with the bond strength in this material. Because the metallic bonding arises from the electrostatic attractive force between the conduction electrons and the positively charged metal ions, the strength of the metallic bond in a metallic substance is dependent on the valence electrons of the metal elements. For the Ce–Fe, Ce–Co, and Ce–Ni compounds, the 3d electrons of the TM elements and some of the 4f and 5d electrons of the Ce elements are conduction electrons. At the same composition, Ce–Fe compound contains relatively less amount of conduction electrons than that of Ce–Co and Ce–Ni. The metallic bonds in Ce–Fe compounds are relatively weaker than those in Ce–Co and Ce–Ni compounds. Hence, the bulk moduli of Ce–Fe compounds are smaller than those of the Ce–Co and Ce–Ni compounds. For Ce–Cu and Ce–Zn compounds, because the valence electrons of Cu and Zn are 4s electrons, the 4f electrons of Ce are localized, the conduction electrons in the Ce–Cu and Ce–Zn compounds are much less than those in the Ce–Fe, Ce–Co and Ce–Zn compounds. As such,

the bond strength in the Ce–Cu and Ce–Zn compounds is weaker than that in Ce–Fe, Ce–Co and Ce–Ni compounds, which can result in relatively smaller bulk moduli.

The shear modulus reflects ability of the material resisting the shear stress, which is correlated with not only the bond strength but also the crystalline structure. For the same crystalline structure, as shown in Table 1, the Ce–Co and Ce–Ni compounds also possess the larger shear moduli. The values of the parameter B/G for Ce–Fe, Ce–Co and Ce–Ni are relatively larger than the critical value of 1.75, which means they are more ductile, while for most phases of Ce–Cu and Ce–Zn compounds the values are smaller than 1.75 so that they are more brittle. The different ductility of some phases of the Ce–Cu and Ce–Zn compounds with those of the Ce–Fe, Ce–Co and Ce–Ni compounds may be due to the different states of the 4f electrons of Ce.

4. Conclusion

We have systematically studied phase stabilities, structures and the electronic properties, as well as mechanical properties of the binary compounds of cerium and 3d-transitional metal systems at ambient pressure and 0 K, using the USPEX code coupled with first-principles calculations. For Ce–Sc, Ce–Ti, Ce–V, Ce–Cr and Ce–Mn systems, no stable crystalline phases are found. For Ce–Fe, Ce–Co, Ce–Ni, Ce–Cu and Ce–Zn binary compounds, besides the experimentally observed phases, a number of new low-energy phases are predicted. The calculated phonon spectrum and elastic constants indicate that all the newly predicted phases are dynamically and mechanically stable. The detailed structures, electronic structures, magnetic properties, and mechanic properties of these structures are computed. The computed electronic structures indicate that there is obvious hybridization between the Ce-4f and Ce-5d states and the TM-3d states in the phases of Ce–Fe, Ce–Co and Ce–Ni compounds. So the Ce atoms in these phases are usually in intermediate valence states between Ce^{+3} and Ce^{+4}. The Ce-4f states in the phases of Ce–Cu and Ce–Zn compounds are much more localized, indicating that the Ce atoms in these phases are in trivalent states. The TM-rich phases of Ce–Fe, Ce–Co, Ce–Ni are usually in ferromagnetic ordering in their ground states, due to the strong exchange interaction between the TM elements. The

Cu-rich and Zn-rich phases of Ce–Cu and Ce–Zn compounds also exhibit magnetic properties where magnetic moments are only located on Ce atoms, due to the Kondo effects. The relative larger bulk moduli indicate that Ce–Co and Ce–Ni compounds have relatively higher ability to resist compression. The computed Pugh parameter B/G suggests that most of Ce–Cu and Ce–Zn compounds may be more brittle because of the more localized states of Ce-4f electrons in the Ce–Cu and Ce–Zn compounds while those of Ce–Fe, Ce–Co and Ce–Ni may be more ductile. Our results offer important new data which will be useful for better understanding of intriguing behavior of Ce 4f electrons in Ce–TM compounds. The predicted new phases of the Ce–TM binary compounds will also motivate future experimental confirmation.

Conflicts of interest

There are no conflicts to declare.

Acknowledgements

References

1 B. Johansson, *Philos. Mag.*, 1973, **30**, 469–482.
2 E. King, J. A. Lee, I. R. Harris and T. F. Smith, *Phys. Rev. B: Condens. Matter Mater. Phys.*, 1970, **1**, 1380.
3 J. W. Allen and R. M. Martin, *Phys. Rev. Lett.*, 1982, **49**, 1106.
4 E. G. Ponyatovskii, *Dokl. Akad. Nauk SSSR*, 1958, **120**, 1021.
5 A. Cadien, Q. Y. Hu, Y. Meng, Y. Q. Cheng, M. W. Chen, J. F. Shu, H. K. Mao and H. W. Sheng, *Phys. Rev. Lett.*, 2013, **110**, 125503.
6 J. M. Léger, *Phys. B*, 1993, **190**, 84–91.
7 H. W. Sheng, H. Z. Liu, Y. Q. Cheng, J. Wen, P. L. Lee, W. K. Luo, S. D. Shastri and E. Ma, *Nat. Mater.*, 2007, **6**, 192–197.
8 Q. S. Zeng, Y. Ding, W. L. Mao, W. Yang, S. V. Sinogeikin, J. Shu, H. K. Mao and J. Z. Jiang, *Phys. Rev. Lett.*, 2010, **104**, 105702.
9 G. Seyfarth, A. S. Rüetschi, K. Sengupta, A. Georges, D. Jaccard, S. Watanabe and K. Miyake, *Phys. Rev. B: Condens. Matter Mater. Phys.*, 2012, **85**, 205105.
10 H. L. Luo, M. B. Maple, I. R. Harris and T. F. Smith, *Phys. Lett. A*, 1968, **27**, 519–520.
11 Y. Ōnuki and T. Komatsubara, *J. Magn. Magn. Mater.*, 1987, **63**, 281–288.
12 M. B. Tang, H. Y. Bai, W. H. Wang, D. Bogdanov, K. Winzer, K. Samwer and T. Egami, *Phys. Rev. B: Condens. Matter Mater. Phys.*, 2007, **75**, 172201.
13 S. V. Streltsov, E. Gull, A. O. Shorikov, M. Troyer, V. I. Anisimov and P. Werner, *Phys. Rev. B: Condens. Matter Mater. Phys.*, 2012, **85**, 195109.
14 F. M. G. N. D. Mathur, S. R. Julian, I. R. Walker, D. M. Freye, R. K. W. Haselwimmer and G. G. Lonzarich, *Nature*, 1998, **394**, 39–43.
15 A. P. Murani, S. J. Levett and J. W. Taylor, *Phys. Rev. Lett.*, 2005, **95**.
16 T. Yamaguchi, N. Ikeda, H. Hattori and K. Tanabe, *J. Catal.*, 1981, **67**, 324–330.
17 M. Ozawa, *J. Alloys Compd.*, 1998, **275**, 886–890.
18 C. A. Luengo, A. L. Cabrera, H. B. MacKay and M. B. Maple, *J. Catal.*, 1977, **47**, 1–10.
19 B. Zhang, D. Q. Zhao, M. X. Pan, R. J. Wang and W. H. Wang, *Acta Mater.*, 2006, **54**, 3025–3032.
20 B. Zhang, D. Q. Zhao, M. X. Pan, W. H. Wang and A. L. Greer, *Phys. Rev. Lett.*, 2005, **94**, 205502.
21 S. F. Matar, *Prog. Solid State Chem.*, 2013, **41**, 55–85.
22 C. Becle and R. Lemaire, *Acta Crystallogr.*, 1967, **23**, 840–845.
23 J. G. Park, *Philos. Mag. B*, 1993, **68**, 653–662.
24 P. Krypyakevich and I. I. Zalutskii, *Dopov. Akad. Nauk Ukr. RSR*, 1965, **31**, 54–56.
25 L. Colombo, G. L. Olcese and G. B. Bonino, *Atti Accad. Naz. Lincei, Cl. Sci. Fis., Mat. Nat., Rend.*, 1963, **35**, 53–57.
26 A. C. Lawson, J. M. Lawrence, J. D. Thompson and A. Williams, *Phys. B*, 1990, **163**, 587–590.
27 H. Asmat, B. Barbara and D. Gignoux, *J. Solid State Chem.*, 1977, **22**, 179–184.
28 I. Vedel, A. M. Redon, J. M. Mignot and J. M. Leger, *J. Phys. F: Met. Phys.*, 1987, **17**, 849–856.
29 R. A. F. G. E. Brodale, E. P. Norman and J. Floquet, *Phys. Rev. Lett.*, 1986, **56**, 390.
30 B. D. R. M. Loewenhaupt and F. Steglich, *Phys. Rev. Lett.*, 1979, **42**, 1709.
31 K. H. J. Buschow and H. V. Daal, *AIP Conf. Proc.*, 1972, **5**, 1464–1477.
32 E. Gratz, E. Bauer, B. Barbara, S. Zemirli, F. Steglich, C. D. Bredl and W. Lieke, *J. Phys. F: Met. Phys.*, 1985, **15**, 1975–1986.
33 T. M. Seixas and J. M. da Silva, *Phys. B*, 1999, **269**, 362–367.
34 L. Nordström, M. S. S. Brooks and B. Johansson, *Phys. Rev. B: Condens. Matter Mater. Phys.*, 1992, **46**, 3458–3464.
35 C. W. Glass, A. R. Oganov and N. Hansen, *Comput. Phys. Commun.*, 2006, **175**, 713–720.
36 A. R. Oganov and C. W. Glass, *J. Chem. Phys.*, 2006, **124**, 244704.
37 A. R. Oganov, Y. Ma, Y. Xu, I. Errea, A. Bergara and A. O. Lyakhov, *Proc. Natl. Acad. Sci. U. S. A.*, 2010, **107**, 7646–7651.
38 C. H. Hu, A. R. Oganov, Q. Zhu, G. R. Qian, G. Frapper, A. O. Lyakhov and H. Y. Zhou, *Phys. Rev. Lett.*, 2013, **110**, 165504.
39 Q. Li, Y. Ma, A. R. Oganov, H. Wang, H. Wang, Y. Xu, H. K. Mao and G. Zou, *Phys. Rev. Lett.*, 2009, **102**, 175506.

40 Y. L. Li, S. N. Wang, A. R. Oganov, H. Gou, J. S. Smith and T. A. Strobel, *Nat. Commun.*, 2015, **6**, 6974.

41 J. F. l. G. Kresse, *Phys. Rev. B: Condens. Matter Mater. Phys.*, 1996, **54**, 11169.

42 J. P. Perdew, K. Burke and M. Ernzerhof, *Phys. Rev. Lett.*, 1996, **77**, 3865–3868.

43 O. Eriksson, L. Nordström, M. S. S. Brooks and B. Johansson, *Phys. Rev. Lett.*, 1988, **60**, 2523.

44 L. Nordström, O. Eriksson, M. S. S. Brooks and B. Johansson, *Phys. Rev. B: Condens. Matter Mater. Phys.*, 1990, **41**, 9111.

45 A. Togo and I. Tanaka, *Scr. Mater.*, 2015, **108**, 1–5.

46 M. Born and K. Huang, *Dynamical Theory of Crystal Lattices*, Clarendon press, 1954.

47 D. Liu, X. Dai, X. Wen, G. Qin and X. Meng, *Comput. Mater. Sci.*, 2015, **106**, 180–187.

48 Z. J. Wu, E. J. Zhao, H. P. Xiang, X. F. Hao, X. J. Liu and J. Meng, *Phys. Rev. B: Condens. Matter Mater. Phys.*, 2007, **76**, 054115.

49 R. Golesorkhtabar, P. Pavone, J. Spitaler, P. Puschnig and C. Draxl, *Comput. Phys. Commun.*, 2013, **184**, 1861–1873.

50 S. J. Kennedy, P. J. Brown and B. R. Coles, *J. Phys.: Condens. Matter*, 1993, **5**, 5169–5178.

51 J. Heyd, G. E. Scuseria and M. Ernzerhof, *J. Chem. Phys.*, 2003, **118**, 8207–8215.

52 S. F. Pugh, *London, Edinburgh Dublin Philos. Mag. J. Sci.*, 1954, **45**, 823–843.

53 K. Nassau, L. V. Cherry and W. E. Wallace, *J. Phys. Chem. Solids*, 1960, **16**, 123–130.

54 Y. Khan, *J. Less-Common Met.*, 1974, **34**, 191–200.

55 B. Butler, D. Givord, F. Givord and S. B. Palmer, *J. Phys. C: Solid State Phys.*, 1980, **13**, L743–L746.

56 L. G. Hector and J. F. Herbst, *J. Alloys Compd.*, 2004, **379**, 41–53.